

In situ transmission electron microscopy study of alpha-brass nanoligament formation, microstructure evolution and fracture

Y.I. He,^a Y.J. Yan,^a L.J. Qiao^{a,*} and Alex A. Volinsky^{a,b}

^aCorrosion and Protection Center, Key Laboratory for Environmental Fracture (MOE), University of Science and Technology Beijing, Beijing 100083, People's Republic of China

^bDepartment of Mechanical Engineering, University of South Florida, Tampa, FL 33620, USA

Received 10 May 2011; accepted 28 May 2011

Available online 6 June 2011

In situ transmission electron microscopy (TEM) tensile tests were performed to study alpha-brass nanoligament deformation, phase transformation and fracture. Nanoligament, suitable for in situ TEM studies, formed under a high strain rate by multiple dislocations at the propagating crack tip. Nanoligaments deform by dislocation slip under a high strain rate and a short relaxation time. Under a low strain rate and a long relaxation time, interdiffusion induced alpha- to beta- and gamma-phase transformation. Microcracks nucleated near the gamma-phase/alpha matrix interface. Phase transformation and its effect on alloy nanocrystal fracture were studied.

Published by Elsevier Ltd. on behalf of Acta Materialia Inc.

Keywords: High-resolution transmission electron microscopy (HRTEM); Phase transformations; Nanocrystalline metal; Diffusion; Fracture

Alloy nanomaterials have been developed in recent years with many novel properties and broad applications [1–3]. Unlike single-phase nanomaterials, alloy nanomaterials are vulnerable to many external factors, including heat, radiation, external stress and even visible light [4], which can enhance interdiffusion and phase transformation and hence alter their properties [5,6]. Thus, it is important to study the microstructure evolution and its effects on the properties of alloy nanomaterials. Conventionally, size and strain rate [7,8] are believed to be major factors in determining the deformation and fracture of nanomaterials. However, to the best of our knowledge, the effects of interdiffusion and phase transformation on tensile deformation and fracture in alloy nanomaterials have not been reported. Two obstacles for conducting such research are: (i) fabricating nanoscale samples analogous to their macroscale counterparts, as different preparation methods may yield different results; and (ii) interdiffusion takes a relatively long time, yet conventional in situ tensile tests in a transmission electron microscope (TEM) are always carried out at a faster rate.

Single nanocrystal ligaments (nanoligaments) can be obtained using a large strain rate tensile test in a

TEM [9]. These nanoligaments have identical structures and chemical compositions as the macroscale samples, and thus are suitable for this study. The nanoligament formation mechanism is discussed in this paper.

To overcome the second difficulty, in situ tensile tests in a TEM with a low strain rate and a long relaxation time between loading intervals were performed to allow interdiffusion. Saturated alpha-brass (32 at.% Zn) was chosen as a sample, as it is prone to interdiffusion and phase transformations. Tensile tests with a high strain rate and a short relaxation time were also performed for comparison.

To eliminate the influence of grain boundaries and internal stress, 0.2 mm thick CuZn alloy sheets were vacuum annealed at 500 °C for 2 h and furnace cooled. Under this thermal treatment, the retained equilibrium α -phase is close to saturated solid solution, with an average grain size of 20 μm . The sample was mechanically polished to 100 μm thickness, electro-polished to 50 μm thickness and then cut into 3 \times 5 mm foils suitable for tensile testing inside the TEM, and finally jet-polished until it became perforated in the center. The 30% HNO₃ + 70% C₂H₅OH electro-polishing electrolyte was used at room temperature and 3 V bias, while the 50% H₃PO₄ + 50% C₂H₅OH jet-polishing electrolyte was used at –40 °C and 8 V bias. In situ tensile tests were performed

* Corresponding author. Tel.: +86 10 6233 4499; fax: +86 10 6233 2345; e-mail: lqiao@ustb.edu.cn

using a tensile stage in a JEM100CXII (JOEL, Japan) TEM operating at 100 keV.

Large strain rates were used to form nanoligaments. After the nanoligaments had been formed, a quasi-static load was applied to study their deformation mechanism. With each loading/holding cycle, the ligaments' bright-field images were captured and analyzed. Finally, fractured specimens were carefully cut to $\Phi 3$ size to preserve the fractured nanoligament and high-resolution transmission electron microscopy (HRTEM) characterization was carried out with an FEI Tacnai F20 TEM operating at 120 keV to identify the corresponding microstructure and phase transformation that occurred during the fracture process.

Ligament crack bridging is the major toughening mechanism in metals [10,11]. Mismatched crack planes in adjacent grains were discovered as a major ligament formation mechanism [11]. Unfortunately the ligament formation mechanism within a single grain has not been systematically studied yet. Under large strain rate loading dislocation multi-slips in the crack vicinity induce a notch at the intersection of the slip plane, deformation twins (or cross-slip bands) and the specimen surface (Fig. 1). By measuring characteristic angles from the select area diffraction (SAD) pattern and the bright-field image in Figure 1a, one can identify the slip planes and hence infer the notch formation mechanism. Contrast analysis of the bright-field image also confirmed this mechanism, as shown schematically in Figure 1c.

Due to the notch stress concentration, microcracks will nucleate preferentially at the notch (Fig. 1b) and propagate through the thinned area between the deformation twins (or cross-slip bands), thus forming a parallelogram crack. Then, accompanied by dislocation activity along its sides, this parallelogram crack becomes blunt, forming a ligament in between adjacent cracks. If the strain rate is low enough, the ligament will be thinned to the submicron- or nanoscale. Figure 1d is a nanoligament sketch.

Due to the above formation mechanism, the slip-induced nanoligaments will have the same chemical composition as the matrix and a similar structure except for the central part, which can be either deformation twins or cross-slip bands. After formation, the ligaments will

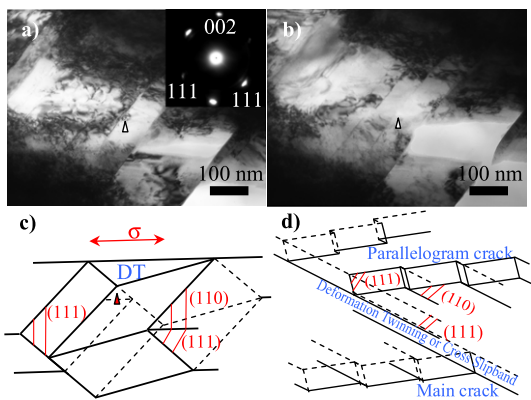


Figure 1. Large strain rate deformation (a) before and (b) after microcrack initiation. The inset shows the corresponding SAD pattern; (c) schematic diagram of the surface notch induced by multi-slip in (a); (d) schematic diagram of the nanoligament formation mechanism.

deform as independent structures. Therefore, in situ fabricated nanoligament is suitable for this study.

Nanowire deformation under tension has been thoroughly studied [12–14]. After nanoligament formation, deformation is localized in the nanoligament as an individual structure, separate from the rest of the sample. Figure 2 shows a typical nanoligament deformation process. Parallel black stripes in the nanoligament are slip bands inherited from the rest of the sample. With increasing strain, the original slip bands disappeared and new slip bands emerged, accompanied by parallel slip steps (Fig. 2b). This implies that the nanoligament deforms by dislocation slip. Multiple repeated nanoligaments tensile tests showed the same deformation mechanism. Although it is challenging to precisely control the nanoligament size, which may affect the deformation mechanism, this result is reasonable considering that deformation twinning will be replaced by dislocation plasticity below the critical sample size [15].

As dislocations in the central slip band gradually slipped out of the structure, the microcrack became blunter, and then the whole structure fractured (Fig. 2c and d). Dislocations in the side-slip bands were still connected to the matrix, so were not starved. This phenomenon is similar to mechanical annealing, which indicates that progressive activation and exhaustion of dislocation sources in source-limited deformation induces hardening [16]. As a result of the impeded plasticity and the relatively large strain rate, stress in the nanoligament will definitely increase and finally induce fracture. Although mechanical annealing was initially discovered in a compression test, this paper shows that it also happens in tensile tests. Dislocation activity governed the plasticity and a mechanical annealing phenomenon was observed in the tensile deformation of nanoligaments, although there was no obvious interdiffusion-induced phase transformation.

To allow adequate diffusion time, a low strain rate with a long relaxation time was applied to the ligament in Figure 3. The relaxation time between each loading interval was approximately 24 h. After each loading and relaxation cycle, a bright-field image was captured for subsequent analysis.

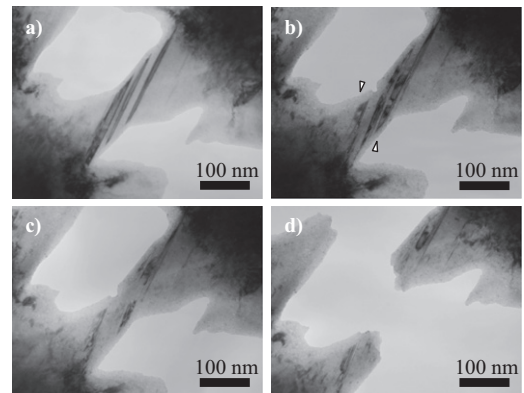


Figure 2. (a–d) The nanoligament deformation fracture process under a large strain rate and a short relaxation time. The arrows indicate slip steps.

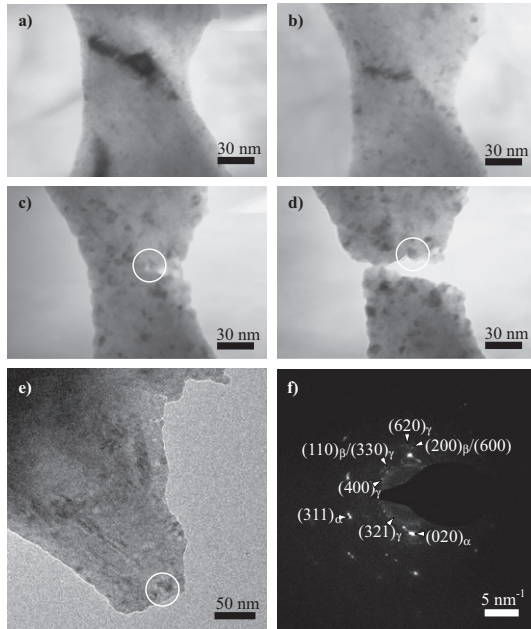


Figure 3. (a–d) The nanoligament fracture process under a low strain rate and a long relaxation time (more than 24 h relaxation between each image). Circles indicate the new phase; (e) select area magnification or SAM and (f) SAD of the fractured nanoligament.

Black spots in the bright-field images can be attributed to local reorientation or phase transformation. The SAD pattern of the ligament (Fig. 3f) proves that phase transformation from the α -phase to the β - and γ -phases (Cu_5Zn_8) occurred. It is important to note that there is some discrepancy in the exact location of the black spot in Figure 3d and e. Since no tilt was applied under both conditions, this is a result of the time delay between the in situ tensile test and the HRTEM characterization, during which diffusion and coalescence might have occurred to minimize the interfacial energy [17]. Figure 4 shows an HRTEM image of the circled black spot in Figure 3e. Lattice parameters can be calculated from its fast Fourier transform (FFT). Comparing the lattice parameters with those of all Cu–Zn alloys, including Cu–O and Zn–O compounds (to exclude the possibility of oxidation), only the $[1\ 4\ 5]$ γ - Cu_5Zn_8 axis matches. Simulated images of γ -

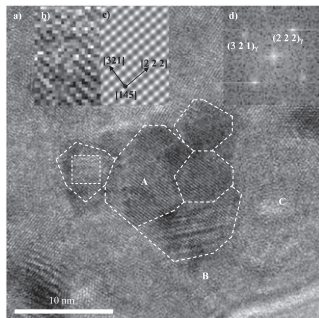


Figure 4. (a) HRTEM image of the black spot indicated by a circle in Figure 3e. Dashed regions indicate subgrains of gamma-brass precipitation; (b) enlarged HRTEM of the white-boxed area in (a); (c) simulated image of γ -CuZn along the $[1\ 4\ 5]$ axis; (d) FFT of the white-boxed area in (a).

Cu_5Zn_8 along the $[1\ 4\ 5]$ axis also agree with the HRTEM image (the simulation parameters are: 120 keV accelerating voltage, 1 mm spherical aberration coefficient, 29 nm specimen thickness and 100 nm defocus). This confirms that the black spot circled in Figure 3 and shown in Figure 4 is γ - Cu_5Zn_8 .

So far, two questions arise:

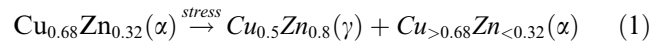
(1) What triggered the phase transformation?

The most influential factors in the in situ TEM tensile test are electron radiation and stress. Based on radiation damage analysis [18,19], displacement effects, electron beam heating and radiolysis can be ignored under a 100 keV accelerating voltage. Referring to the threshold incident energy for the onset of Cu (90 keV) and Zn (40 keV) electron sputtering, sputtering cannot be ignored, and different sputtering rates for Cu and Zn atoms may change the Zn concentration. Calculations based on equations in Egerton et al. [18] show that the sputtering rate for Cu atoms under a 100 keV incident energy is minor, with the sputtering rate for Zn being 15 times larger than that of Cu. Thus, Zn atoms should be more easily removed from the matrix than Cu atoms. The enrichment of Zn in the γ precipitation should not be a result of electron radiation damage.

Previous work has shown that surface atoms diffusion in alloys can be aggregated by radiation [20,21]. Considering that the filament emission and the accelerating voltage were reduced during relaxation to limit the radiation dose, the radiation-enhanced diffusion should be minor. Therefore, the phase transformation in this paper is attributable to stress.

(2) How does stress induce the phase transition?

The transformation from the α - to the γ -phase can be expressed as:



Clearly, the γ -phase has a higher Zn concentration than the α matrix. From the kinetics viewpoint, the transformation must result from the diffusion and segregation of Zn atoms. In this case, there were two Zn sources. First is Zn diffusion from inside out. Higher stress will increase the vacancy concentration throughout the structure. Atom diffusion from inside out should be a major contributor to the increased number of vacancies. Because the diffusion of Cu or Zn in brass is a vacancy-assisted process [22] and the Zn diffusion coefficient in brass is larger than that of Cu [23,24], Zn would concentrate on the surface. The sputtering effect will also increase the Zn concentration on the existing surface. The second source is the surface itself. Because of stress and radiation, the diffusion of surface atoms will be enhanced [25]. Considering the simple model of an atom and vacancy pair, Fick's first law gives the diffusion flux of element i as:

$$J_i = X_i \cdot D_i \cdot \frac{\partial C_i}{\partial x} \quad (2)$$

in which X_i is the atomic percent and $\frac{\partial C_i}{\partial x}$ is the concentration gradient, which is constant in this simple model. If the flux ratio equals the concentration ratio, the composition will not change. However, based on above result,

$$\frac{J_{\text{Cu}}}{J_{\text{Zn}}} = \frac{X_{\text{Cu}} \cdot D_{\text{Cu}}}{X_{\text{Zn}} \cdot D_{\text{Zn}}} < \frac{C_{\text{Cu}}}{C_{\text{Zn}}} \quad (3)$$

The Zn concentration will fluctuate with time and the number of surface sites, leaving some Zn-rich and Zn-depleted surface sites. Overall, stress and a minor sputtering effect triggered reaction (1). Thermodynamically, the specimen's Gibbs free energy can be expressed as:

$$\Delta G = \Delta_r G_m + \Delta\gamma + \Delta\Gamma + \Delta E \quad (4)$$

in which $\Delta_r G_m$ represents the change of Gibbs free energy in reaction (1) under vacuum and at room temperature, $\Delta\gamma$ represents the change in surface energy, $\Delta\Gamma$ represents the γ/α -phase interfacial energy and ΔE is the elastic energy change:

$$\Delta E = -\sigma \cdot \Delta V \quad (5)$$

As the molar volume of the γ -phase is more than 10 times larger than that of the α -phase, the volume expansion ΔV resulting from the above reaction will greatly reduce ΔE and ΔG . In other words, the new phase is stabilized by the applied tensile stress.

Note that the black spot circled in Figure 3 grows with increasing loading/holding cycle time. The HRTEM image in Figure 4 indicates that the growing $\gamma\text{-Cu}_5\text{Zn}_8$ phase consists of five subgrains. The subgrain morphology can be interpreted through effects of deformation [26] and time-delay between in-situ tensile test and HRTEM characterization. Interestingly, as shown in Figure 3c, microcracks initiate preferentially near the interface between the α - and γ -phases. This implies that the $\gamma\text{-Cu}_5\text{Zn}_8$ precipitation is crucial for the nanoligament fracture.

Two major mechanisms can be adopted to interpret this phenomenon. First, Kirkendall voids grow from the interdiffusion process [25,27,28]. Precipitation site A in Figure 4 is in the focal plane, while sites B and C are out of focus. Referring to their contrast in Figure 3d, sites B and C are clearly hollow areas. Considering the interdiffusion, reaction (1) would not only introduce a new phase, but also Kirkendall voids nearby. Therefore, sites B and C are very likely Kirkendall voids. Consequently, the stress level there was higher than elsewhere, resulting in microcrack nucleation. The second mechanism is due to the lower α/γ interfacial strength. Because of the interdiffusion reaction, the vacancy concentration at the α/γ interface will be higher than elsewhere [25,27,28], significantly weakening the interface bond strength. In any case, the interdiffusion reaction inside the alloy nanocrystal significantly reduced the fracture properties.

Through the in situ TEM tensile test and HRTEM characterization, the formation mechanism, deformation and phase transformation in alpha-brass nanoligament has been systematically studied. The phase transformation mechanism has been discussed and the following conclusions have been reached:

1. Multiple dislocation activity due to large strain rate plastic deformation at the crack tip vicinity induces the formation of nanoligaments. These nanoligaments can be used for in situ TEM study of nanoscale deformation and phase transition.
2. Under a large strain rate and short relaxation time loading, nanoligaments deformed by dislocation slip and no interdiffusion-induced phase transformation

was observed. Mechanical annealing occurred before fracture. Under a low strain rate and a long relaxation time, α -phase to β - and γ -phase transformation occurred in the single-crystal ligament. Microcracks nucleated preferentially near the interface between the new γ -phase and the α matrix.

3. The phase transition mechanism identified is reasonable from the viewpoint of thermodynamics and kinetics, considering the interdiffusion and applied stress effects.

This work was supported by the National Natural Science Foundation of China (Grant Nos. 50731003 and 10776001). A.V. would like to acknowledge support from the National Science Foundation.

- [1] Y. Wu, J. Xiang, C. Yang, W. Lu, C.M. Lieber, *Nature* 430 (2004) 61.
- [2] H. Zhu, S. Yang, G. Ni, D. Yu, Y. Du, *Scripta Mater.* 44 (2001) 2291–2295.
- [3] X. Hu, Z. Wang, T. Zhang, X. Zeng, W. Xu, J. Zhang, J. Yan, J. Zhang, L. Zhan, *Appl. Surf. Sci.* 254 (2008) 3845–3848.
- [4] R. Naik, R. Ganesan, K.V. Adarsh, K.S. Sangunni, V. Takats, S. Kokenyesi, *J. Non-Crystalline Solids* 355 (2009) 1939–1942.
- [5] J. Diao, K. Gall, M.L. Dunn, *Nat. Mater.* 2 (2003) 656.
- [6] H.S. Park, *Nano Lett.* 6 (2006) 958.
- [7] Y.H. Wen, Z.Z. Zhu, R.Z. Zhu, *Comput. Mater. Sci.* 41 (2008) 553.
- [8] H. Ikeda, Y. Qi, T. Cagin, K. Samwer, W.L. Johnson, W.A. Goddard Johnson III, *Phys. Rev. Lett.* 82 (1999) 2900.
- [9] Y. He, L.J. Qiao, J.X. Li, W.Y. Chu (in preparation).
- [10] J.K. Shang, R.O. Ritchie, *Metall. Trans. A* 20A (1989) 897.
- [11] K.S. Chang, *Micromechanics of ligament toughening*, *Metall. Trans. A* 22A (1991) 2021.
- [12] H. Zheng, S.X. Mao, *Nat. Commun.* 1 (2010) 144.
- [13] X.D. Han, K. Zheng, Z. Zhang, Z.L. Wang, *Adv. Mater.* 00 (2007) 1.
- [14] H.S. Parks, K. Gall, J.A. Zimmerman, *J. Mech. Phys. Solids* 54 (2006) 1862.
- [15] Q. Yu, Z.W. Shan, J. Li, X.X. Huang, L. Xiao, J. Sun, E. Ma, *Nature* 463 (2010) 335–338.
- [16] Z.W. Shan, R.K. Mishra, S.A. Syed Ashif, O.L. Warren, A.M. Minor, *Nat. Mater.* 7 (2007) 115–119.
- [17] M.J. Yacaman, C.G. Wing, M. Miki, D.Q. Yang, K.N. Piyakis, E. Sacher, *J. Phys. Chem. B* 109 (2005) 9703–9711.
- [18] R.F. Egerton, P. Li, M. Malac, *Micron* 35 (2004) 399.
- [19] Y. Xu, L. Shi, Q. Li, *Micron* 42 (2011) 290.
- [20] R.A. Arndt, R.L. Hines, *J. Appl. Phys.* 32 (1961) 1913.
- [21] S.M. Myers, S.T. Picraux, *J. Appl. Phys.* 46 (1975) 4774.
- [22] H.B. Huntington, F. Seitz, *Phys. Rev.* 61 (1942) 315–325.
- [23] A. D Smigelskas, E.O. Kirkendall, *Trans. AIME* 171 (1947) 130–142.
- [24] W.J. Chen, T.K. Tsai, *Appl. Surf. Sci.* 253 (2007) 6749.
- [25] H.J. Fan, M. Kenz, U. Gosele, *Nano Lett.* 7 (2007) 993.
- [26] Y.B. Wang, B.Q. Li, M.L. Sui, S.X. Mao, *Appl. Phys. Lett.* 92 (2008) 011903.
- [27] S.H. Kim, B.K. Park, *Mater. Lett.* 64 (2010) 938–941.
- [28] J.G. Wang, M.L. Tian, T.E. Mallouk, H. Moses, W. Chan, *Nano Lett.* 4 (2004) 1313–1318.